



Theses and Dissertations

2019-08-01

Comparison of Heat Generation Models in Finite Element Analysis of Friction Welding

Richard Verile Livingston
Brigham Young University

Follow this and additional works at: <https://scholarsarchive.byu.edu/etd>



Part of the [Engineering Commons](#)

BYU ScholarsArchive Citation

Livingston, Richard Verile, "Comparison of Heat Generation Models in Finite Element Analysis of Friction Welding" (2019). *Theses and Dissertations*. 7686.

<https://scholarsarchive.byu.edu/etd/7686>

This Thesis is brought to you for free and open access by BYU ScholarsArchive. It has been accepted for inclusion in Theses and Dissertations by an authorized administrator of BYU ScholarsArchive. For more information, please contact scholarsarchive@byu.edu, ellen_amatangelo@byu.edu.

Comparison of Heat Generation Models in Finite Element Analysis of Friction Welding

Richard Verile Livingston

A thesis submitted to the faculty of
Brigham Young University
in partial fulfillment of the requirements for the degree of
Master of Science

Tracy W. Nelson, Chair
Michael P. Miles
Carl D. Sorensen

Department of Mechanical Engineering
Brigham Young University

Copyright © 2019 Richard Verile Livingston
All Rights Reserved

ABSTRACT

Comparison of Heat Generation Models in Finite Element Analysis of Friction Welding

Richard Verile Livingston
Department of Mechanical Engineering, BYU
Master of Science

Finite element models of friction welding can be used to estimate internal conditions of welds which are useful for weld analysis and developing experimental welding procedures. Many modeling techniques are used to accomplish these goals, each with relative strengths and weaknesses. A comparative analysis of friction welding models using different heat generation methods is presented. The three different heat generation methods examined were viscoplastic friction, constant steady-state generation, and experimentally measured power data. The models were compared against each other using three output measurements: temperature, axial force, and upset. The friction model predicted temperatures within 40°C . Temperature accuracy improved at a higher upset rate and higher spindle speed, when weld samples heated up faster. The model was excellent at predicting upset, with accuracy within 1.5%. Maximum force was predicted within 9-18%. The constant heat generation model typically predicted temperatures within 30°C . Upset was estimated within 7%. Maximum force was predicted within 12% at high feed rates, but accuracy dropped to 28% when feed rate was reduced. The motor power model was the most accurate model at estimating temperature, with a typical accuracy within 25°C . Axial upset was predicted within 5%. Maximum force was predicted within 1-8%, with greater accuracy occurring at higher feed rates.

Keywords: friction welding, finite element, FEA, Inconel 718, heat source, modeling

TABLE OF CONTENTS

LIST OF TABLES	iv
LIST OF FIGURES	iv
NOMENCLATURE	vii
Chapter 1 Introduction	1
Chapter 2 Methods	5
2.1 Experimental Welds	5
2.2 Viscoplastic Friction Model	5
2.3 Heat Generation Models	6
2.3.1 Constant Heat Generation	7
2.3.2 Motor Power Loss	8
2.4 Comparison of the Models	9
Chapter 3 Results and Discussion	10
3.1 Experimental Data	10
3.2 Comparison of Models	11
3.2.1 Temperature	11
3.2.2 Upset	14
3.2.3 Axial Load	15
Chapter 4 Conclusion	18
REFERENCES	20
Appendix A Experimental Data Results	21
A.1 Weld 1	21
A.2 Weld 2	22
A.3 Weld 3	24
Appendix B Model Simulation Results	26
B.1 Weld 1	26
B.2 Weld 2	27
B.3 Weld 3	29

LIST OF TABLES

2.1 Experimental Weld Parameters 5

LIST OF FIGURES

1.1	The four stages of the friction welding process. Source: D’Alvise [1].	1
1.2	In Coulomb friction, shear stress increases linearly with applied load. In plastic flow, shear stress is constant and independent of normal load. Friction welding is believed to exhibit Coulomb friction in its early stages before transitioning to plastic flow. Source: Maalekian [2]	2
1.3	The deformation regions within a friction weld, as proposed by Midling [3]. Z_{cs} represents location of the thixotropic contact region, Z_{pl} the fully plasticized region, and Z_{pd} the partially plasticized region.	3
2.1	The 2-dimensional (left) and 3-dimensional (right) models used to simulate welding with friction-based heating.	6
2.2	The three stages of friction welding: heating, steady state, and cooling. The temperature at the weld interface is approximated as constant during the steady state stage. Source: Midling [3].	7
3.1	Thermocouple (left) and power (right) data collected from Weld 1 and the output curves that were fit to the data.	10
3.2	Different in maximum temperature values at multiple locations of the weld. Maximum temperature error from this work is plotted with errors calculated from similar work.	11
3.3	The temperature mean absolute error, according to model type and set of weld parameters. The motor power model had the least average error and the friction model had the greatest average error.	12
3.4	Experimental and friction model temperatures 2 mm from the weld interface. The friction model predicts temperatures to rise faster than observed experimentally.	13
3.5	Error in predicting final (left) and mean absolute error (right) of upset.	14
3.6	Regression analysis between upset error and temperature error. No statistically significant effect was observed (p-value: 0.77), indicating the upset error probably isn’t directly affected by temperature error in the models.	14
3.7	Maximum force error for all models and weld parameters. Error is expressed as an absolute value and a percent of maximum measured force	15
3.8	Mean absolute error of axial load. Units are given in MPa because they are scalable to other sample sizes, unlike force.	16
3.9	Error of force vs error in temperature during the steady state periods of Weld 1 (top left), Weld 2 (top right), and Weld 3 (bottom).	17
A.1	Experimental data and ”typical” temperature curve at 1 mm (left) and 2 mm thermocouples (right). Data are from Weld 1.	21
A.2	Experimental data and ”typical” temperature curve at 3 mm (left) and 4 mm thermocouples (right). Data are from Weld 1.	21
A.3	Experimental data and ”typical” value curves for axial force (left) and welder motor power (right). Data are from Weld 1.	22
A.4	Experimental data and ”typical” temperature curve at 1 mm (left) and 2 mm thermocouples (right). Data are from Weld 2.	22

A.5	Experimental data and "typical" temperature curve at 3 mm (left) and 4 mm thermocouples (right). Data are from Weld 2.	23
A.6	Experimental data and "typical" value curves for axial force (left) and welder motor power (right). Data are from Weld 2.	23
A.7	Experimental data and "typical" temperature curve at 1 mm (left) and 2 mm thermocouples (right). Data are from Weld 3.	24
A.8	Experimental data and "typical" temperature curve at 3 mm (left) and 4 mm thermocouples (right). Data are from Weld 3.	24
A.9	Experimental data and "typical" value curves for axial force (left) and welder motor power (right). Data are from Weld 3.	25
B.1	Experimental and simulated temperature data for thermocouples positioned 1 mm (left) and 2 mm (right) from the weld interface. Data are for Weld 1.	26
B.2	Experimental and simulated temperature data for thermocouples positioned 3 mm (left) and 4 mm (right) from the weld interface. Data are for Weld 1.	26
B.3	Experimental and simulated data collected for axial force (left) and axial upset (right). Data are for Weld 1.	27
B.4	Experimental and simulated temperature data for thermocouples positioned 1 mm (left) and 2 mm (right) from the weld interface. Data are for Weld 2.	27
B.5	Experimental and simulated temperature data for thermocouples positioned 3 mm (left) and 4 mm (right) from the weld interface. Data are for Weld 2.	28
B.6	Experimental and simulated data collected for axial force (left) and axial upset (right). Data are for Weld 2.	28
B.7	Experimental and simulated temperature data for thermocouples positioned 1 mm (left) and 2 mm (right) from the weld interface. Data are for Weld 3.	29
B.8	Experimental and simulated temperature data for thermocouples positioned 3 mm (left) and 4 mm (right) from the weld interface. Data are for Weld 3.	29
B.9	Experimental and simulated data collected for axial force (left) and axial upset (right). Data are for Weld 3.	30

NOMENCLATURE

a	Thermal diffusivity
δ_{new}	New displacement
δ_{old}	Old displacement
F	Axial force
k	Stiffness
P	Power
p	Pressure
ρc	Volume heat capacity
q_0/A	Net heat flux
T_0	Initial temperature
T_{max}	Maximum Temperature
τ	Torque
μ	Friction coefficient
v_{max}	Maximum surface velocity
ω	Spindle speed (RPM)
Z_{cs}	Thixotropic contact region of a friction weld
Z_{pl}	Fully plasticized region of a friction weld
Z_{pd}	Partially plasticized region of a friction weld

CHAPTER 1. INTRODUCTION

Friction welding is a solid-state welding process made up of four major stages [1]:

1. One workpiece is held in place as the other is rotated at a desired speed (Fig. 1.1(a)).
2. The two workpieces are brought together and heated by friction between the two surfaces (Fig. 1.1(b)).
3. The pieces are at a desired temperature below the melting point and exhibit viscoplastic behavior. The workpieces are upset into each other and eventually come to rest as input energy is removed and the remaining kinetic energy is dissipated into heat and plastic deformation flow. This step is also known as forging (Fig. 1.1(c)).
4. The workpieces are fully at rest and cool down. The weld is complete (Fig. 1.1(d)).

Finite element models can be used to estimate internal conditions in friction welding. Outputs such as material flow and strain rate may be difficult or inconvenient to measure during experimental welds but can be calculated using a model. Models also have the ability to estimate values such as temperature at any location instead of being limited to discrete points. Accurate models

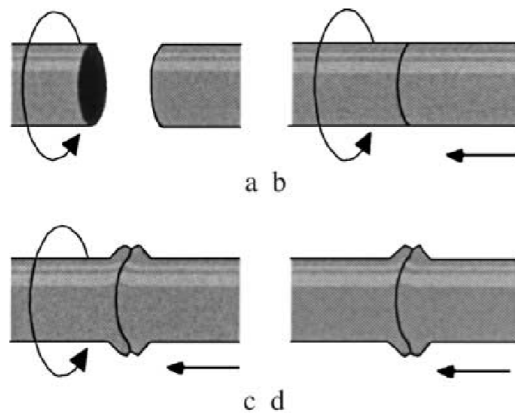


Figure 1.1: The four stages of the friction welding process. Source: D'Alvise [1].

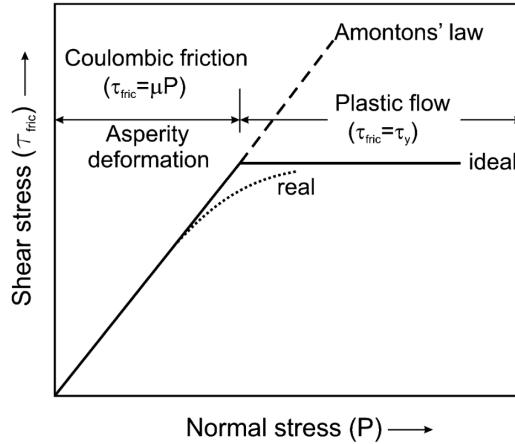


Figure 1.2: In Coulomb friction, shear stress increases linearly with applied load. In plastic flow, shear stress is constant and independent of normal load. Friction welding is believed to exhibit Coulomb friction in its early stages before transitioning to plastic flow. Source: Maalekian [2]

of friction welding can save researchers significant time developing new processes, as procedures can be fine tuned computationally before experimental welds are conducted.

Any model is bound to have shortcomings and limitations, as assumptions and approximations are made to simplify calculations. Some model weaknesses may include the inability to predict weld outputs accurately over certain ranges of input parameters. Sometimes a model may be ineffective at predicting a specific type of weld output altogether. Consequently, many types of models have been developed to overcome the weaknesses of other models.

One method of modeling friction welding uses Coulomb friction between workpieces to generate the heat which facilitates welding [1,4]. Generating heat with Coulomb friction limits the versatility of the model because the coefficient of friction is an empirical term that does not fully represent the steady-state material interaction at the weld interface. The Coulomb friction model assumes that shear stress increases linearly with applied force, which is true for the early stages of welding. However, thermal softening leads to plastic material flow at the weld interface, and shear stress is independent of normal force during plastic flow (Fig. 1.2).

Midling et al. [3] proposed that the weld interface is a shallow, high temperature, thixotropic region caused by high shear strain rates. Under steady state welding conditions, the contact region experiences near-zero friction forces, constant heat generation, constant temperature, and constant axial load. As a thixotropic material, the contact layer experiences viscosity between surfaces of

quired to match experimental temperature profiles. Temperature was modeled very closely, matching experimental temperature nearly identically during warm-up and estimating maximum temperature within 8%.

Maalekian et al. [2] conducted a direct comparison of four different heat sources in a finite element model of orbital friction welding: Coulomb friction, sliding-sticking friction, experimentally measured power data, and an inverse heat conduction approach. The models which utilized a frictionless heat source were found to yield more accurate temperature profiles than friction-based models. Only temperature outputs of the models were compared, ignoring other outputs such as axial force and upset. The models were analyzed for only one set of input parameters.

The objective of this work is to construct three different heat source models of friction welding: Viscoplastic friction, heat source with constant heat generation, and heat source with experimental motor power. Each heat source model was evaluated for strengths and limitations at estimating outputs such as temperature, upset, and axial load. Experimental welds of Inconel 718 were carried out using three different sets of input parameters so possible effects of changing input parameters on model accuracy may be observed.

CHAPTER 2. METHODS

2.1 Experimental Welds

A direct drive rotary friction welder was used to weld two samples of Inconel 718, with each sample measuring 1” in outer diameter, 0.8” in inner diameter, and 4 inches in length. The weld was performed using three different sets of parameters (Table 2.1). Weld 1 was treated as a ”base” set of parameters against which the effects of changing spindle speed (Weld 2) and feed rate (Weld 3) could be compared.

Multiple identical welds were performed at each set of parameters to account for variation in the welding process. Thermocouples were placed on the outside surface of a workpiece at positions 1, 2, 3, and 4 mm away from the initial weld interface. The outputs from the welds were examined and typical expected output values were determined.

Table 2.1: Parameters at which the three experimental welds were conducted. Parameters varied include spindle speed and feed rate.

Weld #	Spindle Speed (RPM)	Feed Rate (mm/s)
Weld 1	1000	2
Weld 2	1250	2
Weld 3	1000	1

2.2 Viscoplastic Friction Model

A 2-dimensional model with viscoplastic friction heating was constructed using FORGE modeling software. The model contains two workpieces whose profiles match those of the experimental workpieces (Fig. 2.1, left). A coefficient of friction between the workpieces was selected to

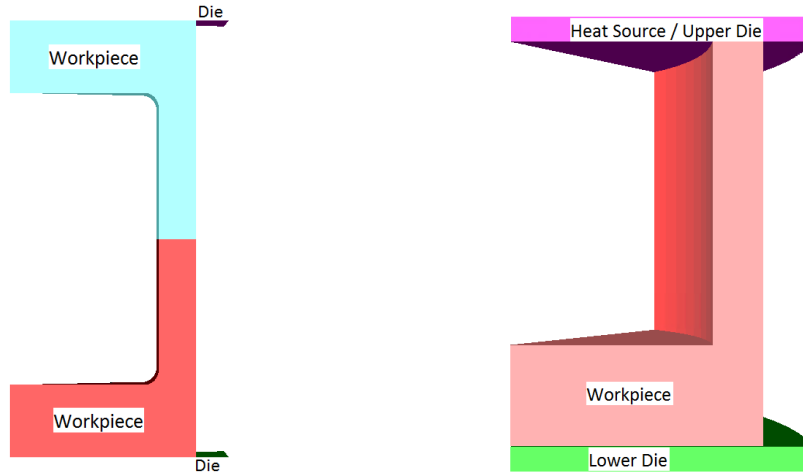


Figure 2.1: The 2-dimensional (left) and 3-dimensional (right) models used to simulate welding with friction-based heating.

bring the expected maximum temperature of the thermocouples to proximity of the experimental maximum temperature values.

In order to incorporate the effects of experimental machine compliance into the model, the welds were initially simulated with infinite machine stiffness. The original displacement was modified to incorporate compliance using the equation:

$$\delta_{new} = \delta_{old} - \frac{F}{k} \quad (2.1)$$

Where δ_{new} is new displacement, δ_{old} is old displacement, F is force, and k is stiffness.

2.3 Heat Generation Models

A 3-dimensional model was constructed using FORGE software (Fig. 2.1, right). The model included a workpiece of the same dimensions of those used in the experimental welds, but cut into a 45° wedge. Planes of symmetry were placed on the cross-sectional faces of the workpiece, allowing the full workpiece to be modeled with 1/8 of the number of nodes and reduced computation time.

A die placed above the workpiece acts as a heat source and represents the weld interface. Sliding friction was included between the workpiece and the die to help represent material flow

without generating significant additional heat. The temperature of the upper die was controlled with time to create desired heat generation profiles. A die placed underneath the workpiece displaced the material at the appropriate feed rate and length of time. The feed rate was halved relative to the experimental feed rate to represent the fact that the model is mirrored symmetrically about the weld interface, so the effective feed rates between the model and experiments are identical.

Compliance within the experimental machine components was incorporated into the model by means of the upper die. The stiffness of the stationary upper die was set to 20 kN/mm, which matches the compliance observed during experiments after accounting for the 1/8 scale wedge of the workpiece and the plane of symmetry at the weld interface.

2.3.1 Constant Heat Generation

The constant heat generation model is based on the model explained by Midling [3], which draws significantly from the work of Rykalin [9]. This model states that welding is composed of three stages: heating, steady state, and cooling (Fig. 2.2).

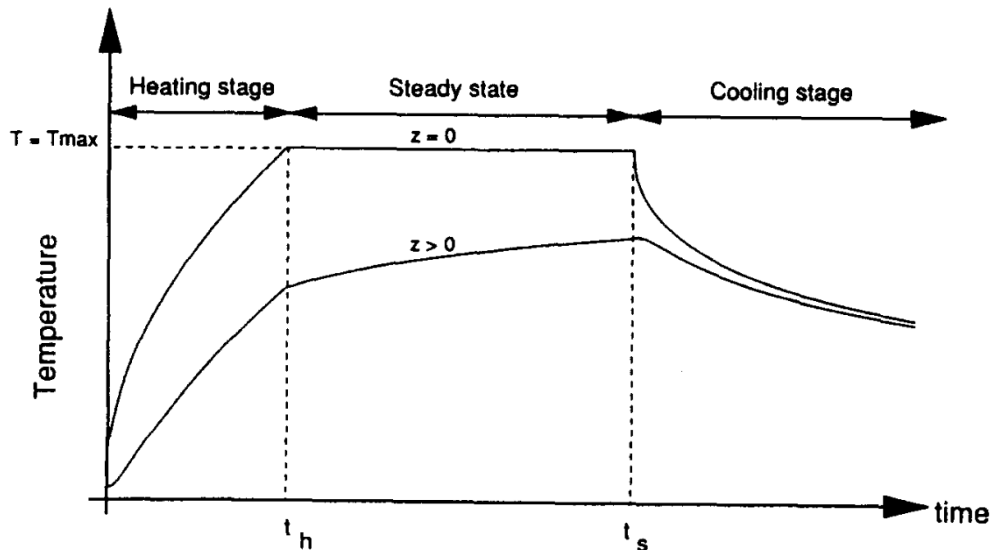


Figure 2.2: The three stages of friction welding: heating, steady state, and cooling. The temperature at the weld interface is approximated as constant during the steady state stage. Source: Midling [3].

During the heating stage, the temperature of the weld interface rises from ambient temperature to the maximum internal temperature of the weld. The time it takes the weld interface to reach maximum temperature can be calculated using the equation:

$$t_h = \left[\frac{(T_{max} - T_0)(\rho c \sqrt{\pi a})}{(q_0/A)} \right]^2 \quad (2.2)$$

where T_{max} is maximum temperature, T_0 is initial temperature, ρc is the volume heat capacity (in $J/mm^3 \text{ } ^\circ C$), a is thermal diffusivity (in mm^2/sec), and q_0/A is net heat flux given by the equation:

$$q_0/A = \frac{2}{3} \mu p v_{max} \quad (2.3)$$

where μ is the friction coefficient, p is pressure (in N/mm^2), and v_{max} is the maximum surface velocity at the outer edge (in m/s).

During the steady state stage, the temperature of the weld interface is assumed to be constant. Therefore, the temperature of the upper die was held constant until the end of the weld when power was removed from the welder motors.

2.3.2 Motor Power Loss

Power loss from the welder motor was measured using the equation:

$$P = \tau \omega \pi / 30 \quad (2.4)$$

where P is power, τ is torque, and ω is spindle speed (RPM).

The resultant power curve was scaled down to 60% because not all of the power used by the motor was efficiently transferred into the workpieces. 60% was chosen as the scaling factor because it was found to bring all three models in agreement with the experimental values. The temperature of the upper die was changed over time to match the power curve within 5% (350 Watts).

2.4 Comparison of the Models

The models were compared to experimental welds based on three outputs: temperature, upset, and axial force. Both maximum and mean absolute error values of these outputs were compared between the models and experiments. Maximum values were compared because they represent the upper limit of values experienced, within which the other output values fall within. Maximum temperature, for example, is relevant because it affects the microstructure of the components. Likewise, maximum upset represents axial shortening and the total amount of material lost during the welding process.

Mean absolute error (MAE) was calculated over the time span of the weld. Mean absolute error is the average error between two continuous measurements and can be used to represent the effectiveness of a model at recreating the conditions present during the welding process. For example, if temperature MAE is low, it can be assumed that heat generation and heat transfer are being accurately represented. On the other hand, if axial force MAE is high, perhaps temperature, compliance, and material flow are not being captured correctly in the model.

CHAPTER 3. RESULTS AND DISCUSSION

3.1 Experimental Data

Temperature, axial loads, motor power, and upset were recorded for each of the welds performed. The data from these tests were used to estimate typical output values for a weld for each set of parameters. Figure 3.1 shows an example of how 'typical' Weld 1 output data was estimated from raw output data. The full compilation of experimental data is found in Appendix A.

Some data curves may be estimates as the available data may be insufficient to precisely measure data values. In particular, this was true in cases where thermocouples became detached from samples or were interfered with by flash coming away from the weld interface. In such cases, 'typical' data curves were estimated using data from adjacent thermocouples including heat rate, cooling rate, and peak temperature time.

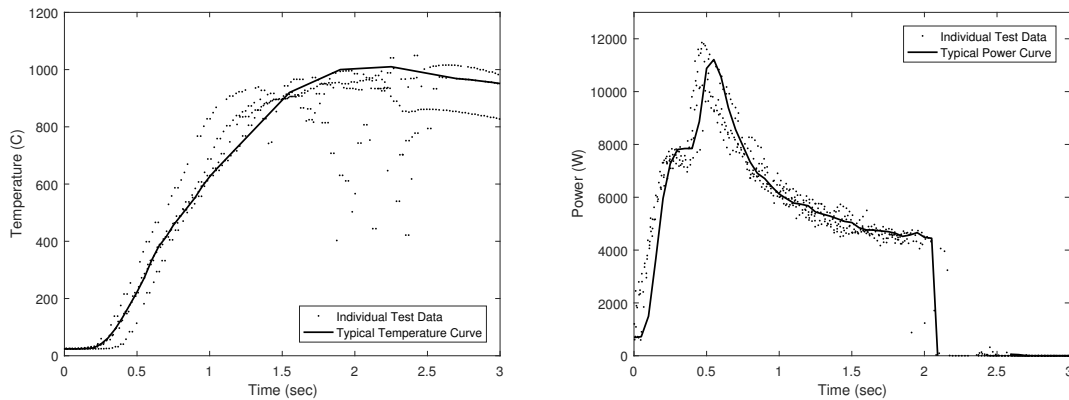


Figure 3.1: Thermocouple (left) and power (right) data collected from Weld 1 and the output curves that were fit to the data.

Experimental motor power was estimated using the measured torque and RPM data from the experiments. The motor power curves were used as the input power values for the power-based heat source model.

3.2 Comparison of Models

A complete collection of model data compared to corresponding experimental data is included in Appendix B. The following section primarily entails the significant findings and analysis derived from the model outputs.

3.2.1 Temperature

Maximum Temperature

All three models estimated the maximum temperatures of the first two thermocouples (1-2 mm from the weld interface) within 1-3.5% (Fig. 3.2). These estimates are on par with the findings in similar work. Wang [6] estimated maximum temperatures within 5% at locations within 1 mm from the weld interface, and Grant [7] estimated maximum temperatures within 2% at points 0.2-1.5 mm from the weld interface.

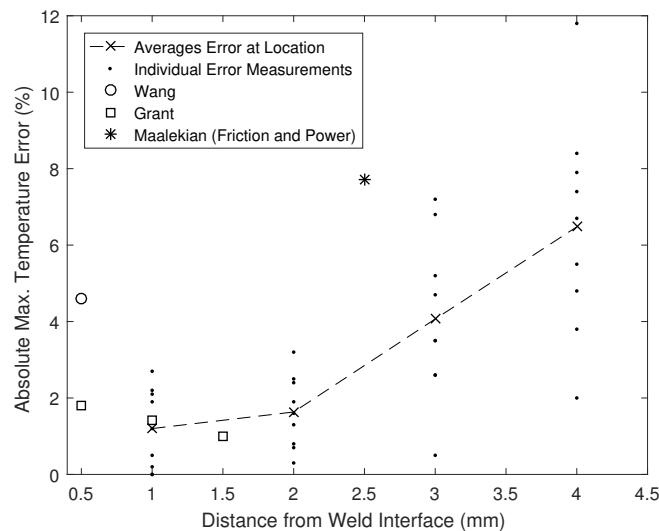


Figure 3.2: Different in maximum temperature values at multiple locations of the weld. Maximum temperature error from this work is plotted with errors calculated from similar work.

Model accuracy decreased as distance from the weld interface increased. The models predicted maximum temperature within 7% at 3 mm from the weld interface and within 12% at 4 mm from the weld interface. Maalekian [2] used the Coulomb friction and motor power models to calculate maximum temperature within 8% at a distance of 2.5 mm from the weld interface. The models in this work estimate maximum temperatures at multiple locations of the weld to comparable levels of accuracy found in other work. This provides validation for the temperatures and heat transfer utilized in this work.

Mean Absolute Error

The motor power model had the least average error for all three sets of weld parameters, estimating temperature typically within 20°C (Fig. 3.3). The constant heat model was the next most accurate model, typically predicting temperature within 26°C. Both the power and constant heat models maintained the same level of accuracy for all three sets of welds, implying that input parameters such as spindle speed and feed rate may not have a significant effect on temperature accuracy for these two models.

The probable reason that the motor power model performed well at estimating temperature is that it is an inverse predictive model. The power fed into the workpieces is directly correlated to

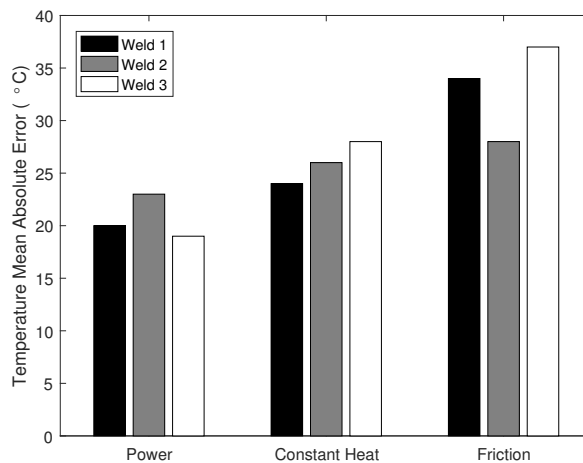


Figure 3.3: The temperature mean absolute error, according to model type and set of weld parameters. The motor power model had the least average error and the friction model had the greatest average error.

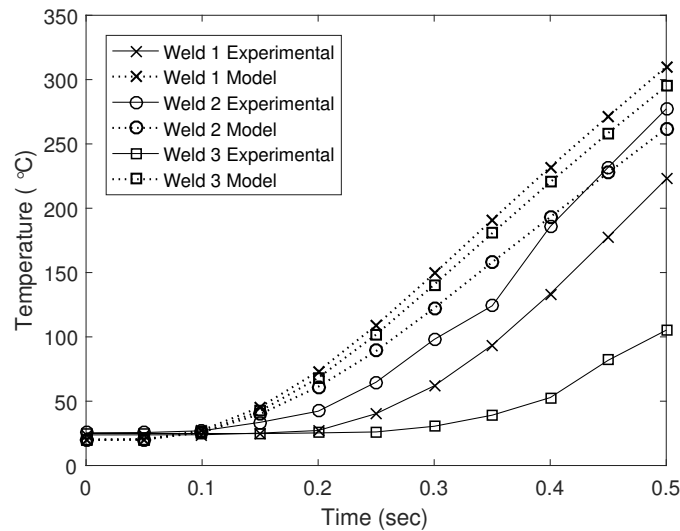


Figure 3.4: Experimental and friction model temperatures 2 mm from the weld interface. The friction model predicts temperatures to rise faster than observed experimentally.

the power used by the experimental welder motor. Thus, the motor power model isn't predictive, as welds must be performed and outputs recorded before the model can be created.

The friction model had the greatest temperature accuracy during Weld 2 and the least accuracy during Weld 3. Maalekian [8] noted that friction models generally predict temperature increases far more rapid than those measured experimentally. This was observed in this work, as Fig. 3.4 shows the experimental and model temperatures for a thermocouple positioned 2 mm from the weld interface.

After 0.5 seconds of welding, the friction models predict temperatures to rise to 260-310°C. Over the same period of time, the experimental thermocouples rose to temperatures ranging from 105-275°C. Weld 2 (high spindle speed, high feed rate) experienced the greatest rate of heating and the greatest temperature MAE accuracy (Fig 3.3) of the friction. Conversely, Weld 3 (low spindle speed, low feed rate) had the slowest heating rate and worst temperature MAE accuracy. From these observations, temperature predictions from friction models are expected to be more accurate as experimental heating rates increase, such as when feed rate and spindle speed are increased.

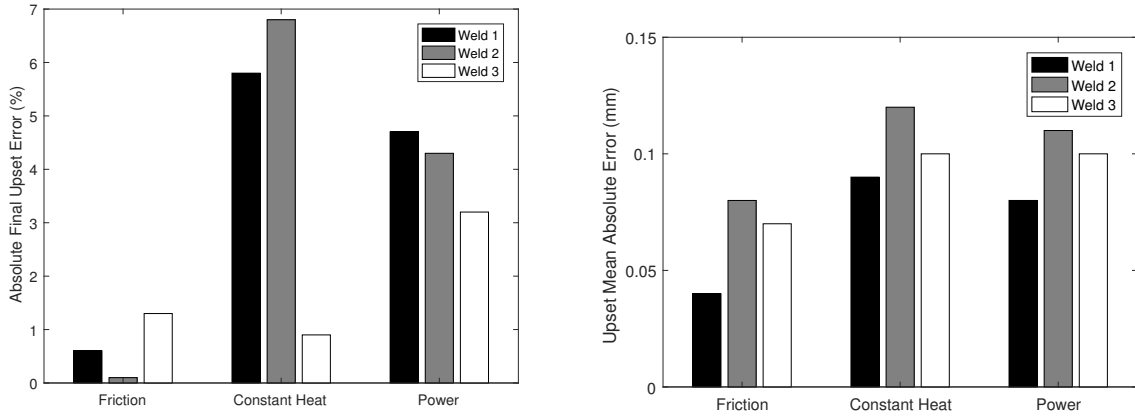


Figure 3.5: Error in predicting final (left) and mean absolute error (right) of upset.

3.2.2 Upset

For all 3 welds, the friction model most accurately predicted material upset (Fig. 3.5). It had an MAE of about 0.08 mm and a final error within 1.3%. Similar levels of accuracy were observed over all three sets of weld parameters.

The constant heat and motor power models predicted final upset within 7% and upset MAE within 0.12 mm. For reference, Grant’s model [7] predicted final upset within 14%. This verifies that the models are within accuracies typically obtained by comparable models.

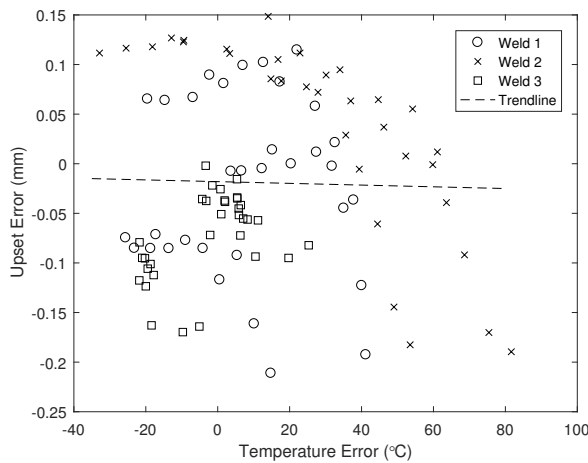


Figure 3.6: Regression analysis between upset error and temperature error. No statistically significant effect was observed (p-value: 0.77), indicating the upset error probably isn’t directly affected by temperature error in the models.

Possible effects of temperature error on upset error were considered. Upset error and temperature error were compared against each other during the decelerating 'cooldown' phase of the welding process. A regression analysis was applied to temperature and upset, and it was found that temperature error does not have a statistically significant effect (p-value: 0.77) on the upset observed in the models (Fig. 3.6).

3.2.3 Axial Load

Maximum Load

The motor power model was the most accurate predictions of maximum force for all three sets of weld parameters (1-8%) (Table 3.7). Accuracy decreased in Weld 3 when feed rate was reduced. This same effect was observed in the constant heat model, which suggests that the two heat source models are best at predicting maximum force at higher feed rates. The constant heat model predicted maximum force within 9-12% at high feed rates before increasing to 28% error when feed rate was reduced.

The friction model predicted maximum force within 9-18%, which is comparable to the accuracies obtained by the constant heat model. The friction model was relatively consistent across the three sets of weld parameters, though error was about 30% less for Weld 1 than in Welds 2 and 3.

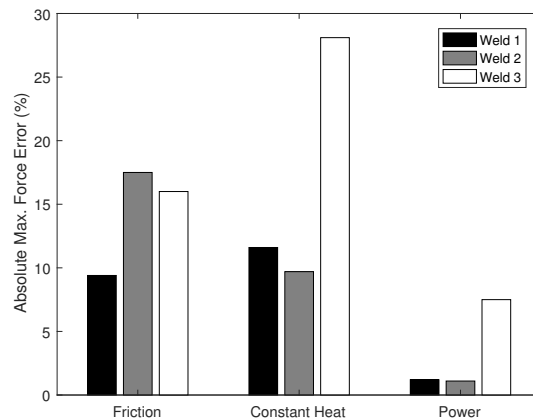


Figure 3.7: Maximum force error for all models and weld parameters. Error is expressed as an absolute value and a percent of maximum measured force

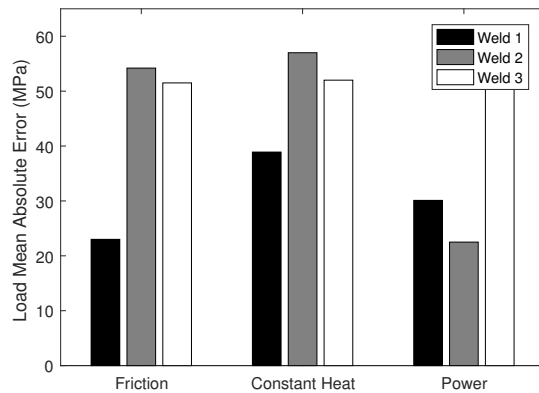


Figure 3.8: Mean absolute error of axial load. Units are given in MPa because they are scalable to other sample sizes, unlike force.

Mean Absolute Error

Comparisons of force MAE doesn't offer many insights into model performance (Fig. 3.8). The three models exhibited some of their best accuracies in Weld 1, with a MAE within 23-38 MPa. When spindle speed increased (Weld 2), the motor power model improved slightly (from 30 to 22 MPa) while error nearly doubled for the friction and constant heat models (from 23/39 MPa to 54/57 MPa). When feed rate was decreased relative to Weld 1, force predictions became less accurate for all three models.

An investigation was made into whether or not temperature error may have influenced axial load error in the models. After all, flow stress can vary significantly with changing temperature. The errors in temperature and axial load during the steady state period of the weld were examined using a regression analysis (Fig. 3.9).

A statistically significant (p-value: <0.001) correlation between temperature and axial load in Weld 2 (Fig. 3.9, top right) supports the idea that temperature errors could be influencing load error in the models. However, the same trend is not observed in Welds 1 and 3. In Weld 1, the friction model shows no statistically significant correlation between errors (p-value: 0.7). In Weld 3, the constant heat and motor power models each showed a positive correlation between temperature error and load error—opposite of the negative correlation expected and observed in Weld 2. Overall, an overarching correlation between temperature and load was not observed. This suggests there are other factors that influence the axial load errors observed in the models.

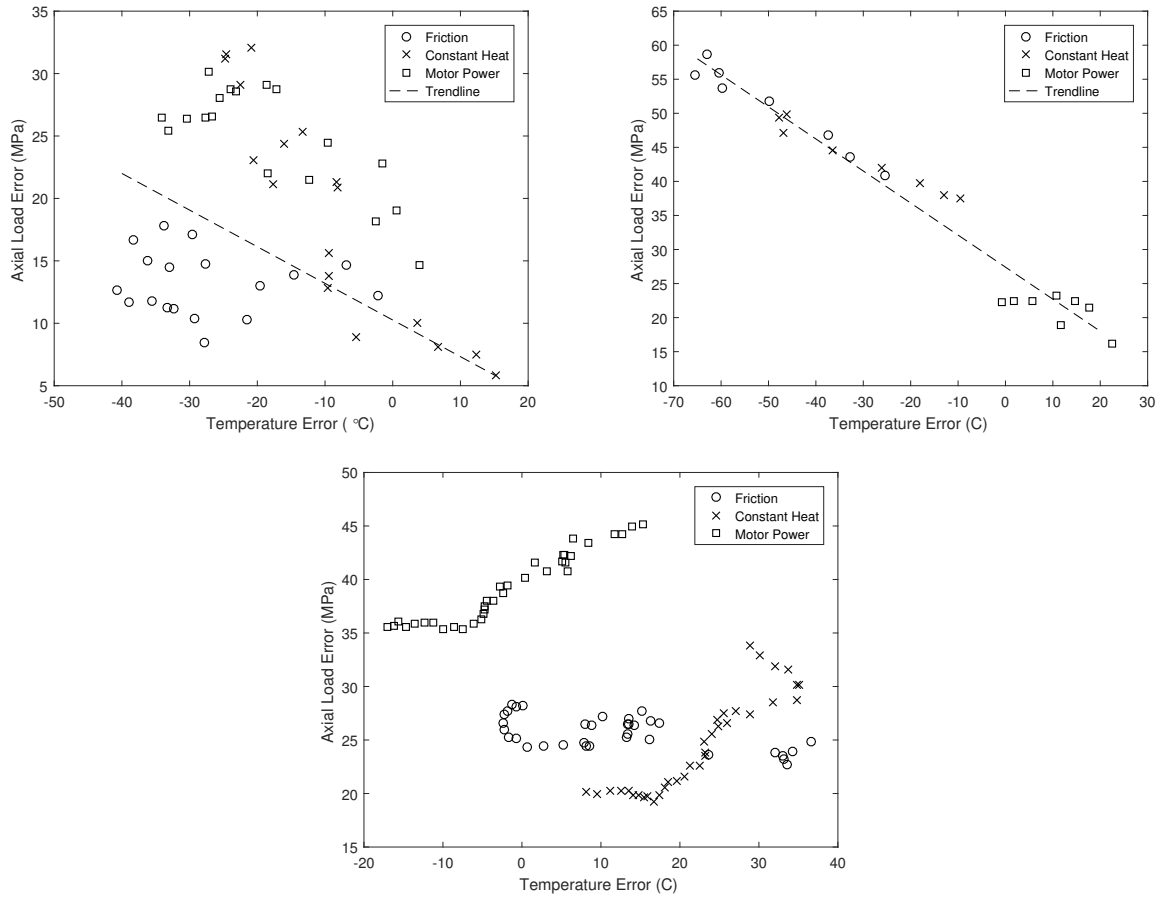


Figure 3.9: Error of force vs error in temperature during the steady state periods of Weld 1 (top left), Weld 2 (top right), and Weld 3 (bottom).

CHAPTER 4. CONCLUSION

Finite element models of friction welding were created using three different methods of heat generation. One method of heat generation was simulating viscoplastic friction between two workpieces. The second method was using a heat source providing constant heat to the workpiece. The final method was using a heat source to input heat flux into the workpiece matching motor power recorded from experimental welds.

The models were designed to replicate welds with three different sets of input parameters. The outputs of the welds—temperature, upset, and axial force—were compared to the corresponding outputs of the finite element models.

None of the models in this work demonstrated the ability to reliably predict weld outputs without the assistance of inverse-predictive practices. Materials in friction welding undergo significant temperature changes, high strain rates, evolving friction laws, dynamic stress-strain relationships, and other intricate properties which are simplified in contemporary models. The ability for models to represent these complex features over a wide range of parameters is not sufficient enough for reliable predictive modeling to be utilized.

The motor power model demonstrated the greatest accuracy at estimating temperature and axial load across all observed weld parameters. However, the input heat flux for the model was derived from measurements obtained from experimental samples. The inverse-predictive nature of the motor power model severely limits its usefulness in situations in which experimental data is not available.

The friction and constant heat models are not necessarily dependent on experimental data for calibration, but still have weaknesses which limit their ability to predict friction welding outputs. This work demonstrated that the friction model's temperature accuracy and the constant heat model's axial load accuracy varied with changing input parameters. The inability of these models

to maintain a consistent accuracy across all weld parameters significantly decreases their overall predictive capabilities.

A summary of model performance follows.

Temperature

1. The friction model typically predicted temperature within 40°C, but accuracy improved to 28°C when spindle speed was increased and the experimental workpieces heated up faster.
2. The constant heat model typically predicted temperatures within 30°C.
3. The motor power model predicted temperatures, on average, within 25°C.

Upset

1. The friction model predicted upset within 0.08 mm and maximum upset within 1.3%.
2. The constant heat model predicted upset within 0.12 mm and maximum upset within 7%.
3. The motor power model predicted upset, on average, within 25°C.

Axial load

1. The friction model estimated maximum force within 18% and average load within 55 MPa.
2. The constant heat model predicted maximum force within 28% and average load within 57 MPa. At high spindle speed and low feed rate, these accuracies improved to 10% and 39 MPa, respectively.
3. The motor power model estimated maximum force within 8% and average load within 50 MPa.

REFERENCES

- [1] Dalvise, L., Massoni, E., and Walløe, S., 2002. “Finite element modelling of the inertia friction welding process between dissimilar materials.” *Journal of Materials Processing Technology*, **125**, pp. 387–391. v, 1, 2
- [2] Maalekian, M., Kozeschnik, E., Brantner, H., and Cerjak, H., 2008. “Comparative analysis of heat generation in friction welding of steel bars.” *Acta Materialia*, **56**(12), pp. 2843–2855. v, 2, 4, 12
- [3] Midling, O., and Grong, Ø., 1994. “A process model for friction welding of Al-Mg-Si alloys and Al-SiC metal matrix composites. I. Temperature and strain rate distribution.” *Acta Metallurgica et Materialia*, **42**(5), pp. 1595–1609. v, 2, 3, 7
- [4] Şahin, M., and Akata, H. E., 2003. “Joining with friction welding of plastically deformed steel.” *Journal of Materials Processing Technology*, **142**(1), pp. 239–246. 2
- [5] Fu, L., Duan, L., and Du, S., 2003. “Numerical simulation of inertia friction welding process by finite element method.” *WELDING JOURNAL-NEW YORK*, **82**(3), pp. 65–S. 3
- [6] Wang, L., Preuss, M., Withers, P., Baxter, G., and Wilson, P., 2005. “Energy-input-based finite-element process modeling of inertia welding.” *Metallurgical and Materials Transactions B*, **36**(4), pp. 513–523. 3, 11
- [7] Grant, B., Preuss, M., Withers, P., Baxter, G., and Rowson, M., 2009. “Finite element process modelling of inertia friction welding advanced nickel-based superalloy.” *Materials Science and Engineering: A*, **513**, pp. 366–375. 3, 11, 14
- [8] Maalekian, M., Kozeschnik, E., Brantner, H. P., and Cerjak, H., 2008. “Finite element modeling of orbital friction welding of eutectoid steel bars.” *Metallurgical and Materials Transactions A*, **39**(4), pp. 844–852. 3, 13
- [9] Rykalin, N., Pugin, A., and Vasil’eva, V., 1959. “The heating and cooling of rods butt-welded by the friction process.” *Weld. Prod.*, **6**, pp. 42–52. 7

APPENDIX A. EXPERIMENTAL DATA RESULTS

A.1 Weld 1

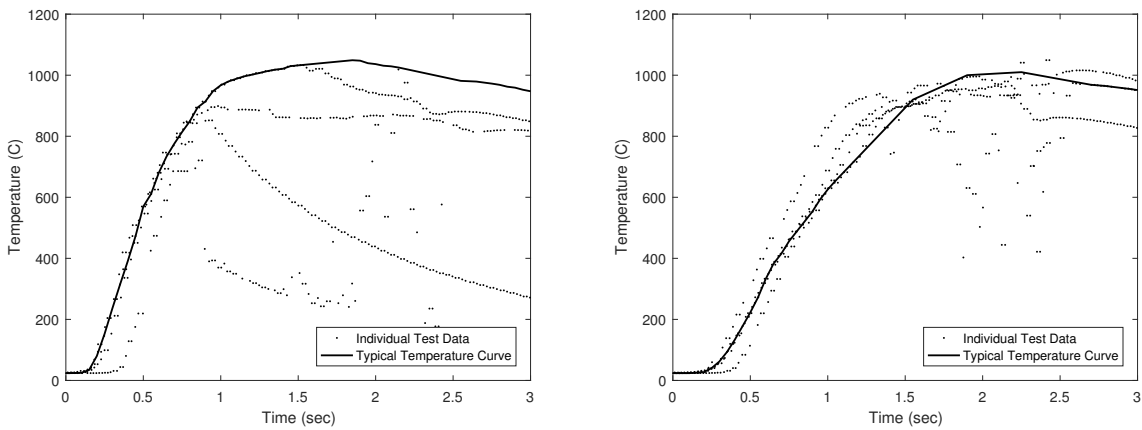


Figure A.1: Experimental data and "typical" temperature curve at 1 mm (left) and 2 mm thermocouples (right). Data are from Weld 1.

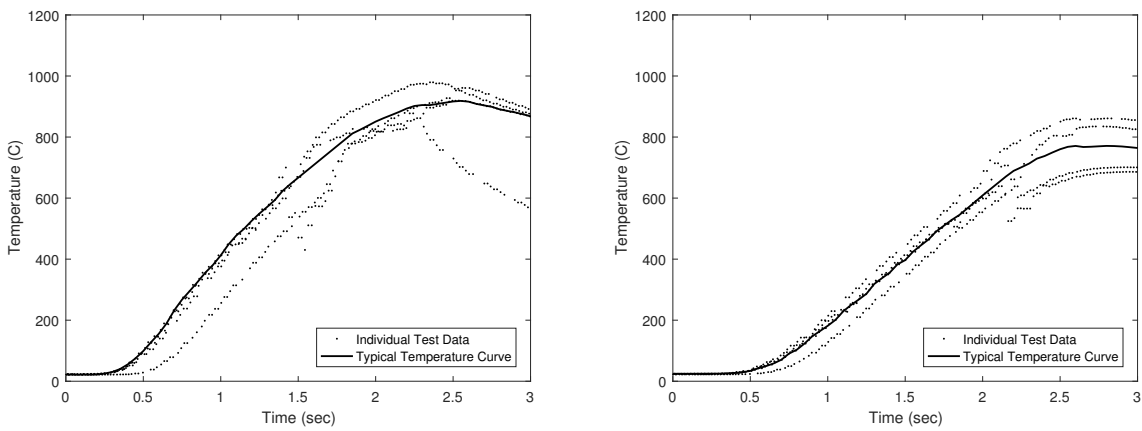


Figure A.2: Experimental data and "typical" temperature curve at 3 mm (left) and 4 mm thermocouples (right). Data are from Weld 1.

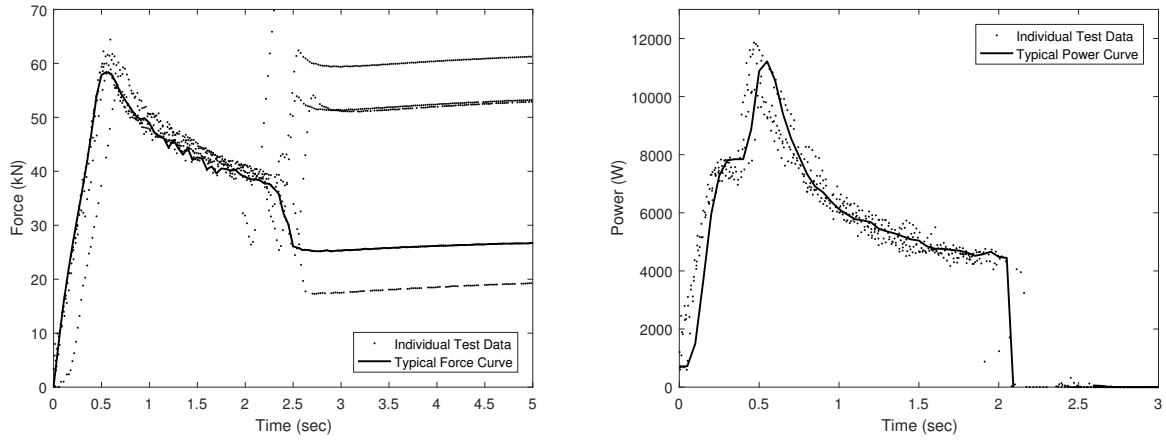


Figure A.3: Experimental data and "typical" value curves for axial force (left) and welder motor power (right). Data are from Weld 1.

A.2 Weld 2

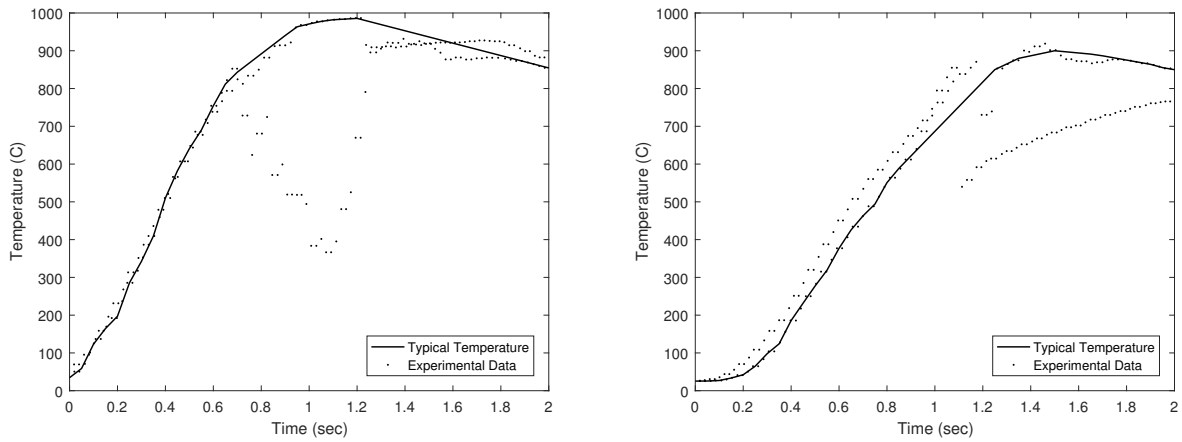


Figure A.4: Experimental data and "typical" temperature curve at 1 mm (left) and 2 mm thermocouples (right). Data are from Weld 2.

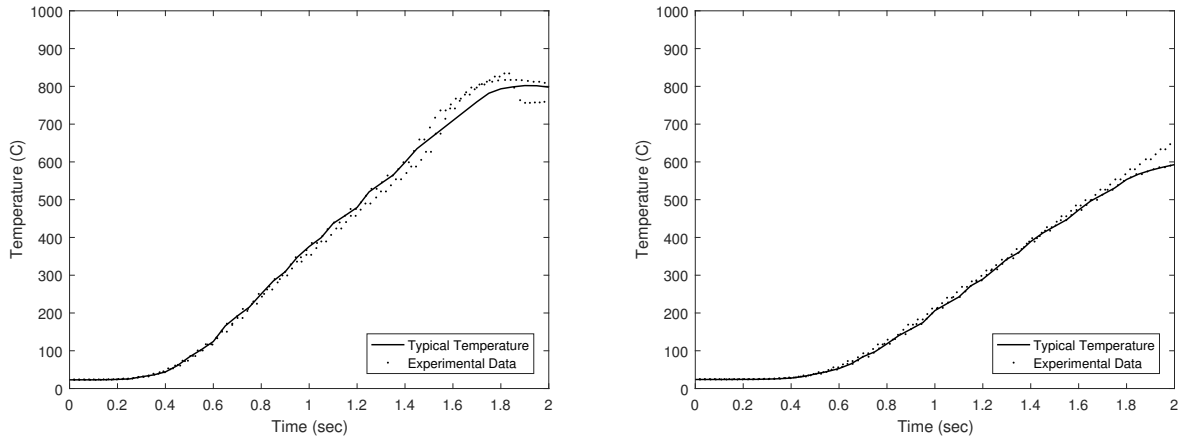


Figure A.5: Experimental data and "typical" temperature curve at 3 mm (left) and 4 mm thermocouples (right). Data are from Weld 2.

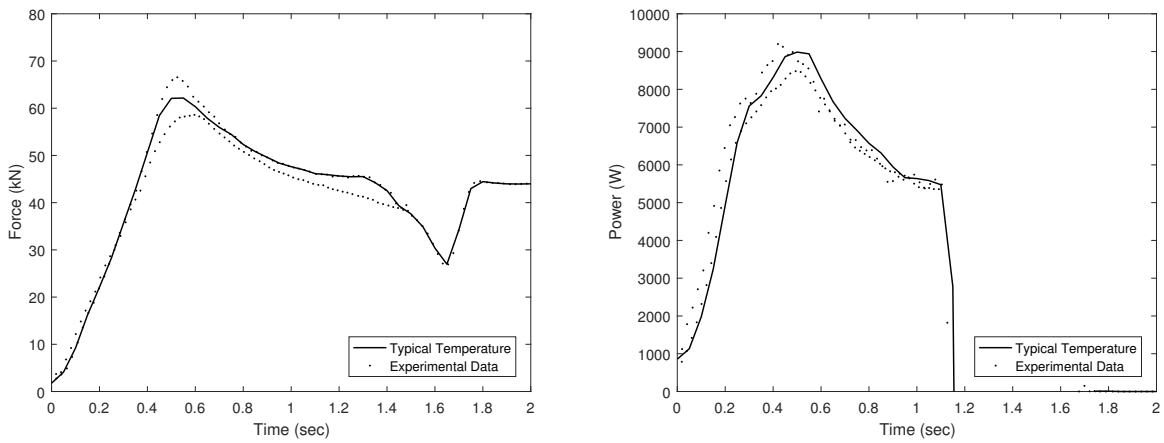


Figure A.6: Experimental data and "typical" value curves for axial force (left) and welder motor power (right). Data are from Weld 2.

A.3 Weld 3

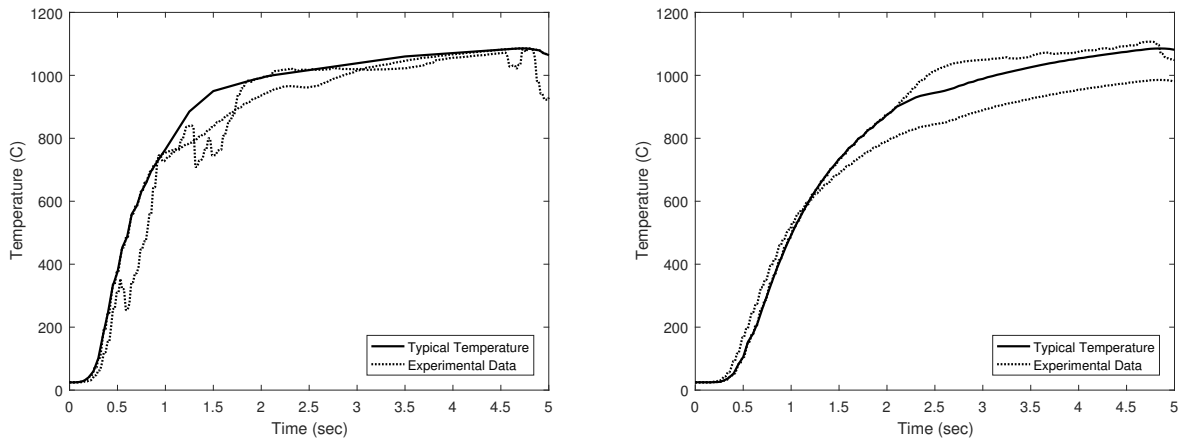


Figure A.7: Experimental data and "typical" temperature curve at 1 mm (left) and 2 mm thermocouples (right). Data are from Weld 3.

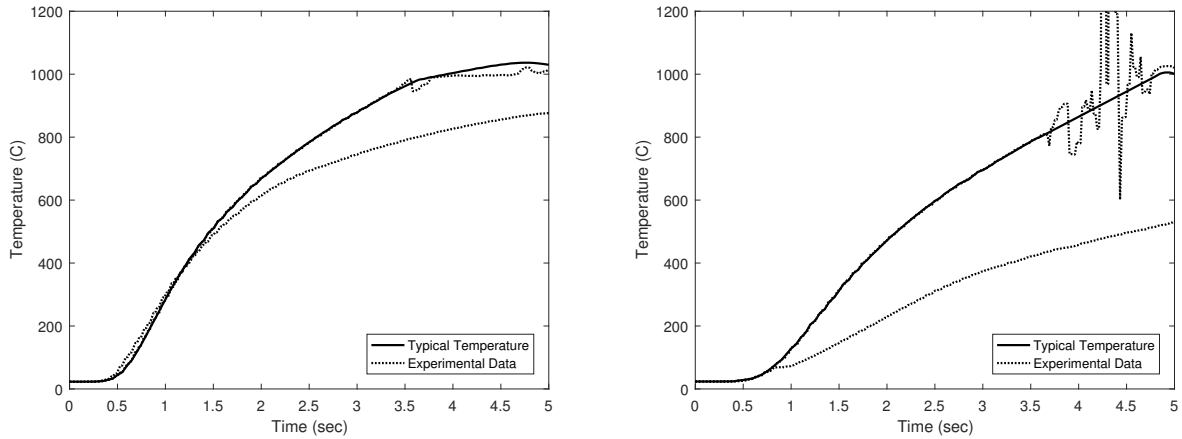


Figure A.8: Experimental data and "typical" temperature curve at 3 mm (left) and 4 mm thermocouples (right). Data are from Weld 3.

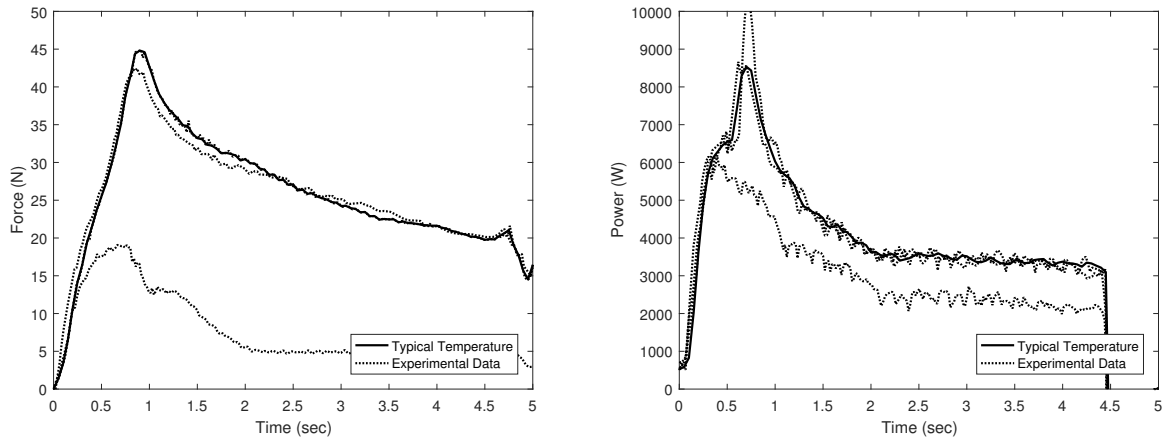


Figure A.9: Experimental data and "typical" value curves for axial force (left) and welder motor power (right). Data are from Weld 3.

APPENDIX B. MODEL SIMULATION RESULTS

B.1 Weld 1

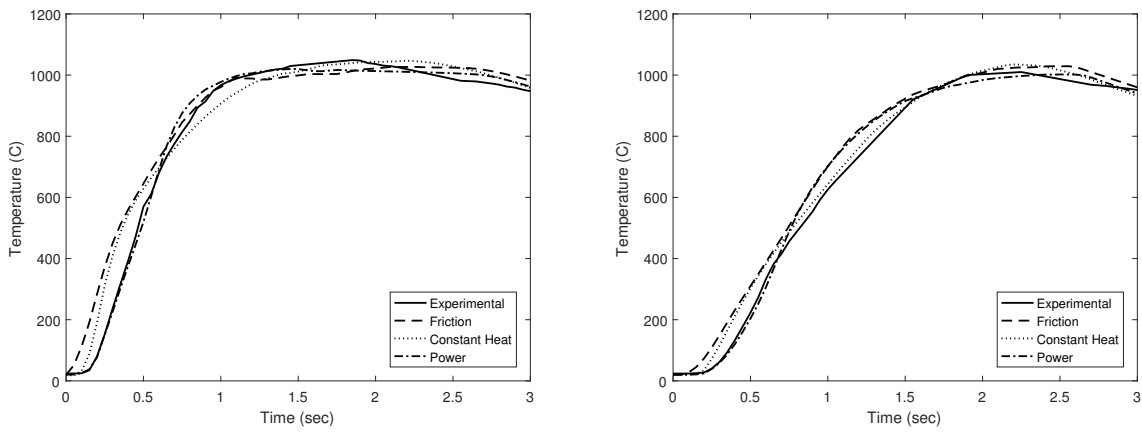


Figure B.1: Experimental and simulated temperature data for thermocouples positioned 1 mm (left) and 2 mm (right) from the weld interface. Data are for Weld 1.

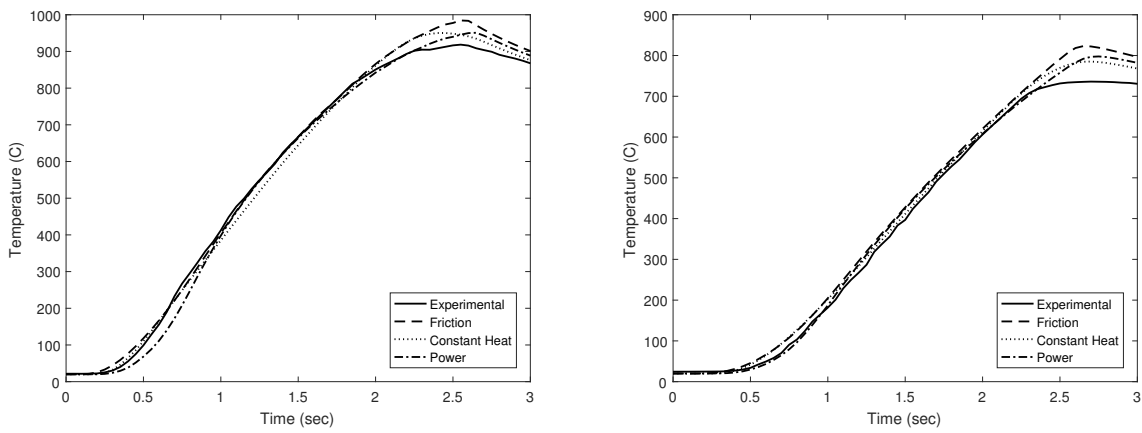


Figure B.2: Experimental and simulated temperature data for thermocouples positioned 3 mm (left) and 4 mm (right) from the weld interface. Data are for Weld 1.

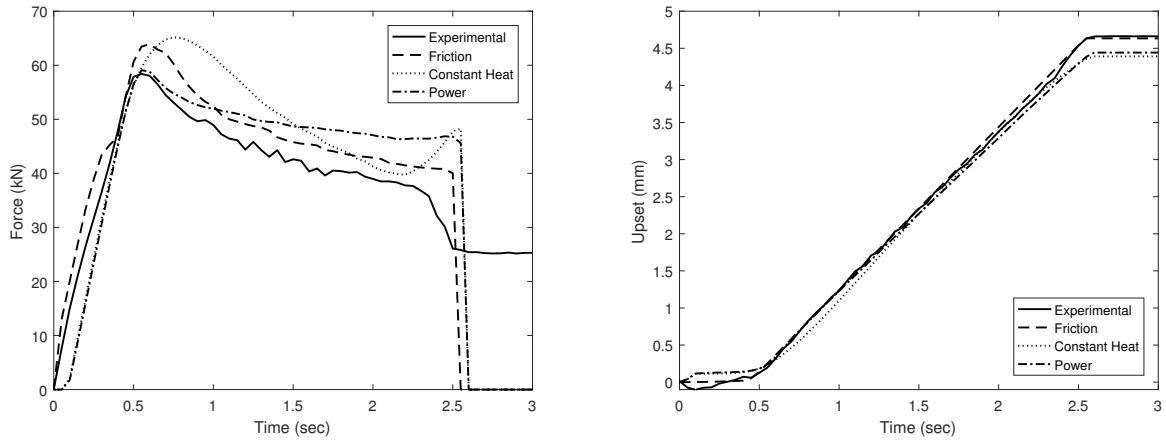


Figure B.3: Experimental and simulated data collected for axial force (left) and axial upset (right). Data are for Weld 1.

B.2 Weld 2

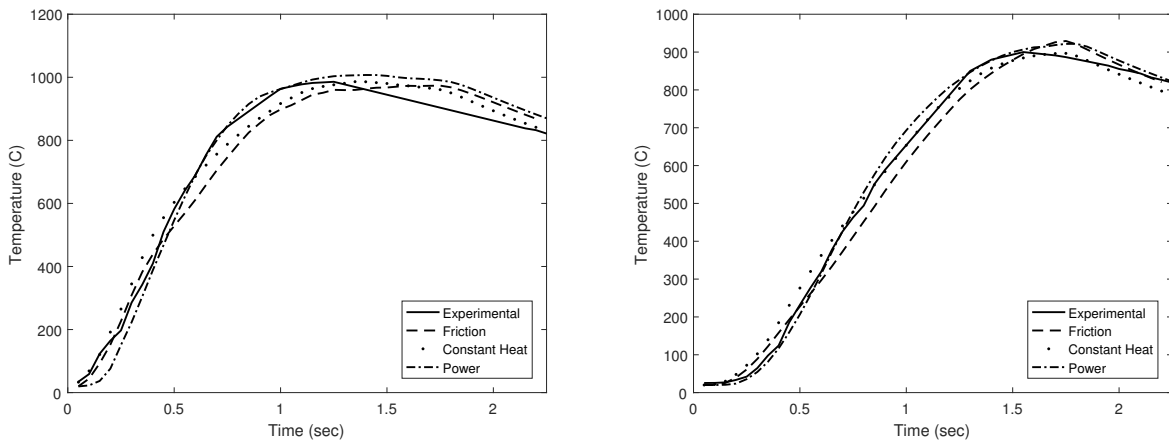


Figure B.4: Experimental and simulated temperature data for thermocouples positioned 1 mm (left) and 2 mm (right) from the weld interface. Data are for Weld 2.

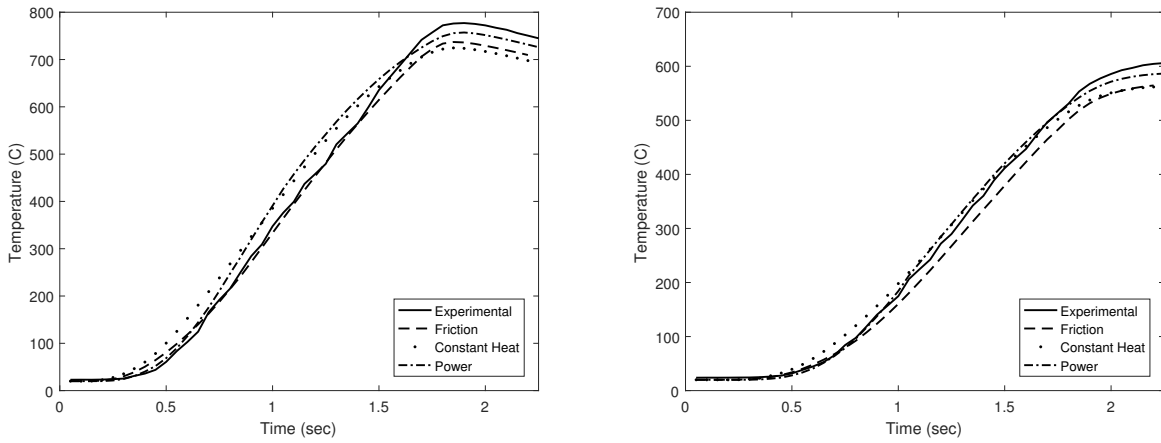


Figure B.5: Experimental and simulated temperature data for thermocouples positioned 3 mm (left) and 4 mm (right) from the weld interface. Data are for Weld 2.

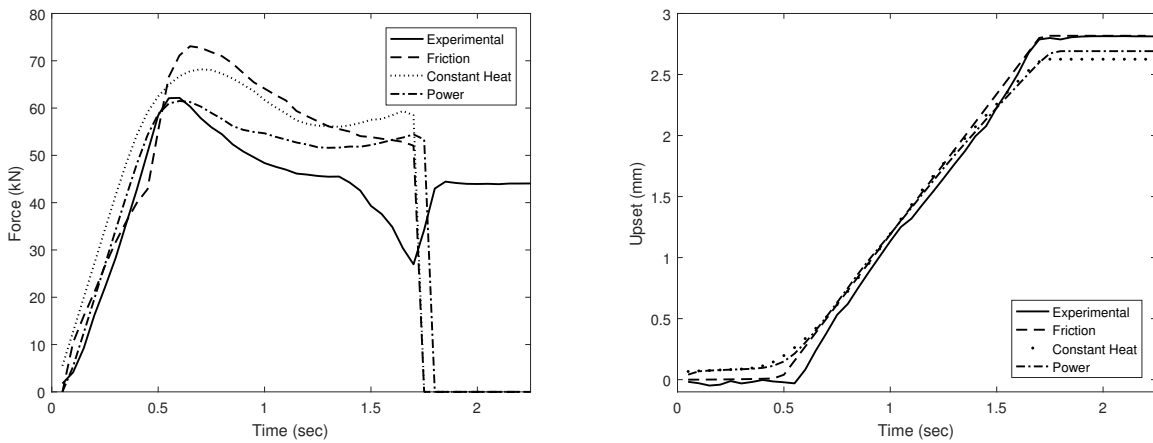


Figure B.6: Experimental and simulated data collected for axial force (left) and axial upset (right). Data are for Weld 2.

B.3 Weld 3

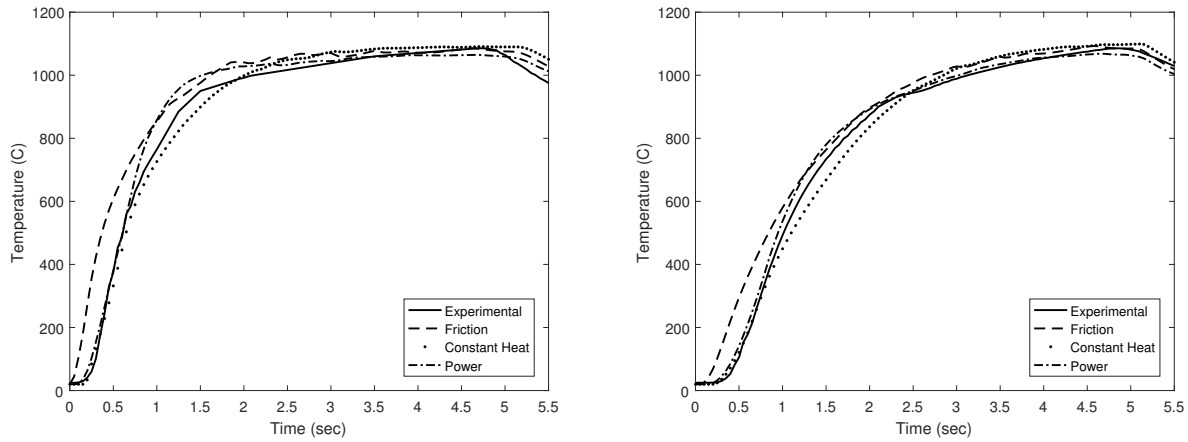


Figure B.7: Experimental and simulated temperature data for thermocouples positioned 1 mm (left) and 2 mm (right) from the weld interface. Data are for Weld 3.

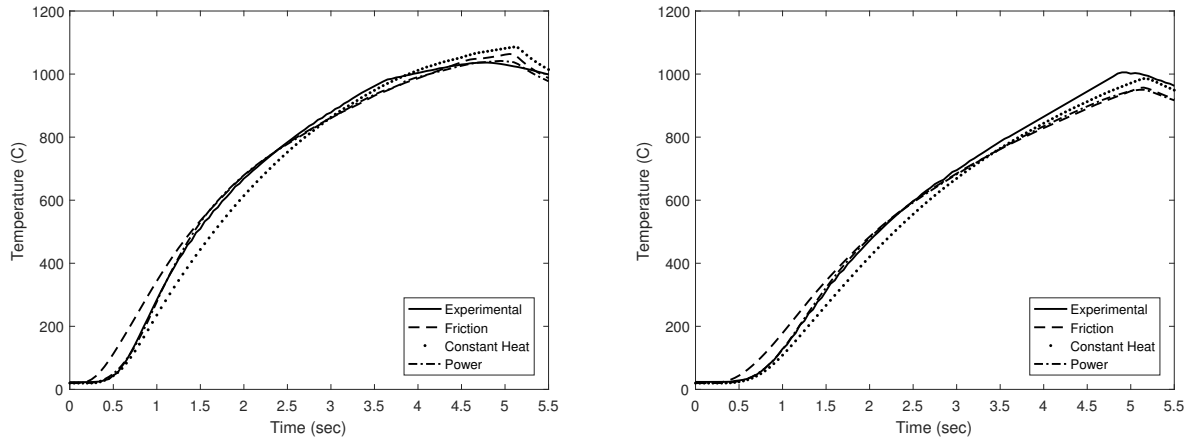


Figure B.8: Experimental and simulated temperature data for thermocouples positioned 3 mm (left) and 4 mm (right) from the weld interface. Data are for Weld 3.

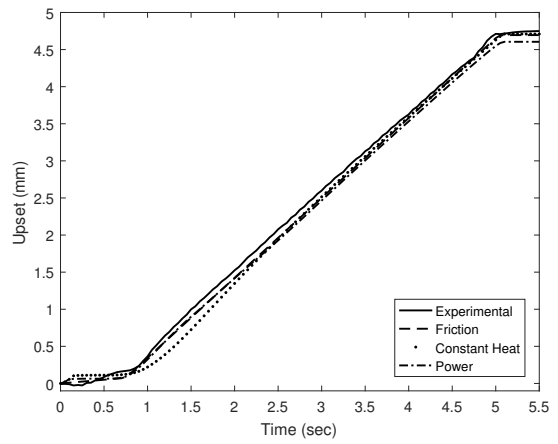
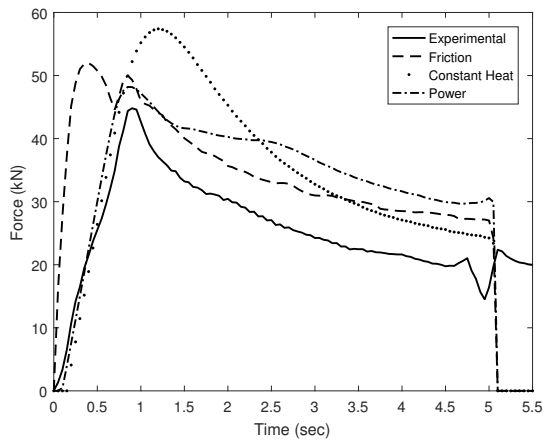


Figure B.9: Experimental and simulated data collected for axial force (left) and axial upset (right). Data are for Weld 3.